Inlet Effects on the Aerodynamics and Acoustics of a Centrifugal Blower

X. Laparra and M.C.M. Wright

ISVR Technical Report No 296

June 2002

University
of Southampton

SCIENTIFIC PUBLICATIONS BY THE ISVR

Technical Reports are published to promote timely dissemination of research results by ISVR personnel. This medium permits more detailed presentation than is usually acceptable for scientific journals. Responsibility for both the content and any opinions expressed rests entirely with the author(s).

Technical Memoranda are produced to enable the early or preliminary release of information by ISVR personnel where such release is deemed to the appropriate. Information contained in these memoranda may be incomplete, or form part of a continuing programme; this should be borne in mind when using or quoting from these documents.

Contract Reports are produced to record the results of scientific work carried out for sponsors, under contract. The ISVR treats these reports as confidential to sponsors and does not make them available for general circulation. Individual sponsors may, however, authorize subsequent release of the material.

UNIVERSITY OF SOUTHAMPTON

INSTITUTE OF SOUND AND VIBRATION RESEARCH

FLUID DYNAMICS AND ACOUSTICS GROUP

**Inlet Effects on the Aerodynamics and
Acoustics of a Centrifugal Blower**

by

X Laparra and M C M Wright

ISVR Technical Report No. 296

June 2002

Authorized for issue by
Professor C L Morfey, Group Chairman

Abstract

This report deals with the CSN (coopération pour le Service National) placement sponsored by the Research Department at Renault, and realized at ISVR (Institute of Sound and Vibration Research), University of Southampton, Great Britain. The subject of this placement was about the aerodynamic and acoustic effects of the air inlet of an automotive centrifugal blower.

Experiments were carried out at LEMFI (Laboratoire d'Energétique et de Mécanique des Fluides Interne), Ecole National Supérieure des Arts et Métiers (ENSAM), France. Seven different inlet geometries were tested with a single blower on the fan rig at ENSAM. In each case, the acoustic (i.e. in-duct sound power) and aerodynamic (i.e. rotational speed, static pressure and flow rate) performances were recorded for eight different flow rates.

These experiments demonstrate the importance of the air inlet geometry: Like any other passive part of the ventilating system it generates a pressure loss as well as a fall-off in the flow rate. The global acoustic power is strongly correlated to the pressure loss, and the geometries that deliver the best aerodynamic performances appear to generate the less acoustic power.

Résumé/Conclusion

Le présent rapport expose les travaux effectués à l'ISVR (Institute of Sound and Vibration Research) de l'université de Southampton (Grande Bretagne) dans le cadre d'une coopération pour le Service National (CSN) pour le compte de la Direction de la Recherche Renault. Cette étude a pour sujet les effets aérauliques et acoustiques d'entrée d'air sur les ventilateurs centrifuges équipant les systèmes de climatisation automobiles.

Des essais ont été menés dans le LEMFI (Laboratoire d'Energétique et de Mécanique des Fluides Interne), à l'Ecole National Supérieure des Arts et Métiers (ENSAM) de Paris. Sept différentes géométries d'entrée d'air ont été testées sur le banc d'essais de l'ENSAM pour un même ventilateur centrifuge. Dans les sept cas et pour huit différents débits ont été mesurés à la fois les performances aérodynamiques (Vitesse de rotation du ventilateur, pression statique et débit délivrés) et acoustiques (puissance acoustique en conduite).

Les résultats obtenus confirment l'importance du choix de l'entrée d'air : d'un point de vue aérodynamique l'entrée d'air génère à la fois une perte de charge et une diminution du débit, comme tout autre élément du circuit de climatisation. Le comportement acoustique en revanche est plus particulièrement propre à l'entrée d'air : La puissance acoustique générée par une source acoustique (le ventilateur) dépend notamment de son chargement (impédance acoustique) en entrée. Les spectres de tiers d'octaves observés sont cependant peu sensibles à l'entrée testée, et conservent globalement des allures très similaires. Quelques disparités apparaissent toutefois, en particulier dans le domaine des basses fréquences. Ces différences ont peu d'effets lorsque l'on exprime la puissance acoustique en dB(A).

Acknowledgements

Content

List of symbols

Ω angular speed of the fan (rad.s^{-1})

N Rotational speed (rpm)

B number of blades

U_{tip} tip velocity (m.s^{-1})

D_2 Impeller diameter (m)

D_c Diameter of the duct of sound pressure measurement (m)

D Diameter of the chamber of static pressure measurement (m)

d Diameter of the diaphragm (m)

r Radial position of the microphones inside the duct (m)

P Acoustic pressure (Pa)

Lp Sound pressure level (dB Re. 2.10^{-5} Pa)

LpA A-weighted sound pressure level (dB(A) Re. 2.10^{-5} Pa)

W Acoustic power (W)

Lw Sound power (dB Re. 10^{-12} W)

LwA A-weighted sound power (dB(A) Re. 10^{-12} W)

T temperature (K)

ΔP Static pressure (Pa)

ρ Air density (kg/m^3)

c sound velocity (m.s^{-1})

M Mach number

Q Flow rate (kg/h)

1. Introduction

This study takes place within a 16 months CSN placement (Coopération pour le Service National) at the Institute of Sound and Vibration Research (ISVR) on behalf of the RENAULT Research Department. The aim of this partnership is to evaluate the effects of the air inlet on the aerodynamic and acoustic performances of a centrifugal blower, as part of the HVAC (Heating, Ventilation, Air Conditioning) automotive system.

A theoretical study previously made on axial fans showed the influence of the velocity profile of the flow impinging the blades on the acoustic power radiated by the fans. Tonal noise is then produced at the blade passage frequency and harmonics. This study must show whether a similar phenomenon happens in the case of centrifugal fans.

The experiments were made during 2 weeks of December 2001 at ENSAM (Ecole National des Arts et Métiers), Paris (France), in the fluid mechanics department LEMFI (Laboratoire d'Energétique et de Mécanique des Fluides Interne). Seven different inlet geometries were tested there with a same centrifugal blower and using the same fan rig. In order to have a better understanding of the aerodynamic and acoustic effects of the air inlet, the tested geometries have basic shapes (bends, straight ducts) and do not pretend to be realistic, although they are inspired by real inlets (bends, cross...).

2. The experimental setup

2.1. Presentation of the fan rig

The fan rig was build according to the European standards ISO 5136 [4] for the acoustic part and ISO 5801 [5] for the aerodynamic one. It is composed of a blower with a specific inlet, a duct of circular cross-section where the measurements take place, and an anechoic

Figure 1 – Scheme of the fan rig

Figure 2 – fan rig – configuration 2 (with adapter)

Figure 3 – fan rig – view of the anechoic termination

termination (to prevent sound reflections from the duct end). All these components (including the blower) are fixed on a firm support.

A rectifier is placed right after the fan outlet, in order to adapt the rectangular fan outlet to the circular inlet of the rig. It verifies $0.95 < \dfrac{\pi d_1^2}{4bh} < 1.07$

where d_1 is the diameter of the circular inlet, and (b,h) the dimensions of the rectangular fan outlet.

Conical transitions are situated between the later rectifier and the measurement duct, and between the measurement duct and the chamber of static measurement (preceding the anechoic termination). The angle of their slope must be smaller than 15°, and the minimum length verifies:

$$\frac{l_{min}}{l_0} \approx \frac{\text{greatest area}}{\text{smallest area}} - 1 \quad \text{with} \quad l_0 = 1\,\text{m}.$$

3

2.2. Instrumentation

All the experiments are made at the same voltage thanks to a power supply providing 12V.

A micro manometer gives the effective pressure delivered by the centrifugal fan.

Three 1/2 inches microphones with turbulence screens are positioned in the same duct cross section, each at a $2\pi /3$ .angular position from the others (Figure 5). They measure

Transducers:
⇒ microphones &
preamplifiers (1 to 4)
⇒ accelerometers (1 to 4)
⇒ intensity probe (1)

Application software:
⇒ dBENV32
Environmental noise
⇒ dBBATI32
Building acoustics
⇒ dBFA32
Real time frequency analysis
and post-processing analysis

HARMONIE box:
Connected to PCCard (PCMCIA)
⇒ High speed serial transmission

Laptop:
⇒ data storage on hard disk
⇒ display and analysis of results

Digital inputs/outputs :
⇒ tachometry signal
⇒ remote control
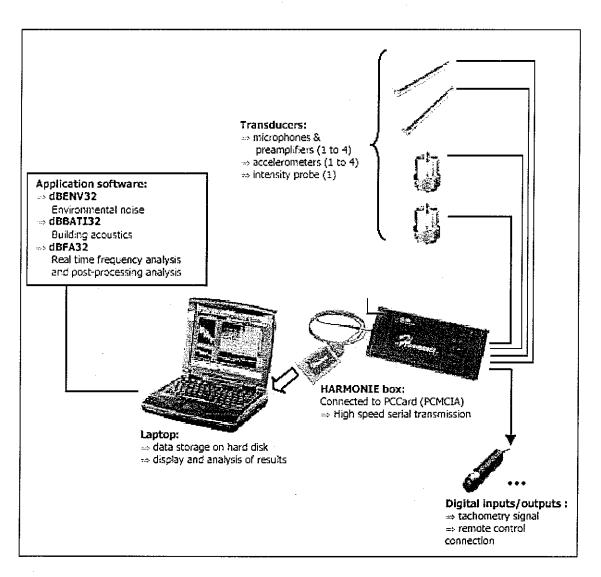connection

Figure 4 – The HARMONIE system

4

the in-duct sound pressure level.

The three microphones are linked to a "HARMONIE" acquisition card provided by the 01dB-Stell company. It allows us to acquire the three channels with a 3201 points resolution in real time. The software dBFA32 (01dB-Stell) that controls the HARMONIE card was unfortunately limiting the card capabilities, and the real time acquisition was not possible with more than two channel simultaneously. The audio signals were then first recorded simultaneously on the three channels and later post processed. The filter bandwidth was 3.125 Hz in all experiments.

The rotational speed of the fan wheel is given by an optical tachometer. This method presents the great advantage of being cheap and accurate enough. It is probably not the best method in our case though, since we need to aim the optical ray at a spot on the wheel: with distorted inlet geometries we can no longer access the wheel with the light beam. With straight inlets (adapter, duct...) we can aim the beam at the wheel, but we need to hold the tachometer in front of the inlet during the speed measurement. This introduces a pressure loss, and modifies the rotational speed of the wheel.

A better way to do would have been to fix a dynamic sensor on the casing and deduce the rotational speed from the frequency spectrum given by the sensor.

While I made the speed measurement with the optical tachometer, I used as well the acoustic spectra of the three microphones to get the rotational speed of the wheel: the frequency of the peaks is proportional to the rotational speed, therefore I used the frequency of the fundamental of the tones created by the spokes of the bowl, and compared it with the rotational speed given by the optical tachometer.

2.3. Method of acquisition

2.3.1. Aerodynamic setup

Since the voltage of the blower is fixed (12 V), the flow rate is modified by the outlet duct cross section: circular diaphragms of multiple diameters (210 to 48 mm) can be fixed on the anechoic termination.

The following parameters are measured:

- T (K) temperature

- ΔP (Pa) static pressure, measured in the chamber that precedes the anechoic termination.

According to the European standard ISO 5801 [5], the flow rate is deduced from the measured static pressure ΔP:

$$Q_m = \alpha \pi \frac{d^2}{4} \sqrt{2\rho \Delta P}$$

where

d (m) diameter of the diaphragm,

$\rho = \dfrac{P}{rT}$ (kg/m^3) air density (assuming the air is a perfect gas), with $P = P_{atm} + \Delta P$, $P_{atm} = 101325$ Pa and $r = 287$ J.kg^{-1}.K^{-1} (for dry air)

and

$$\alpha = A.\left(1 - r_{\Delta P}.\left(B - C.r_{\Delta P}\right)\right)$$

$$A = 0.5993 + 0.1599\beta^2 - 0.9156\beta^4 + 6.5675\beta^6 - 9.1429\beta^8$$

$$B = 0.249 + 0.0701\beta^2 - 0.243\beta^4 + 0.113\beta^6$$

$$C = 0.0757 + 0.058\beta^2 + 0.22\beta^4 + 0.25\beta^6$$

$\beta = \dfrac{d}{D}$, D (m) diameter of the chamber of static pressure measurement (Figure 1).

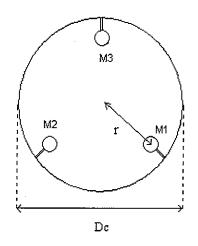$$r_{\Delta P} = \frac{\Delta P}{P_{atm}}$$

6

Figure 5 - Position of the microphones

2.3.2. Acoustic setup

The three microphones are located in the same section of the measurement duct (Figure 5). When only plane waves propagate in the duct, the radiated power can be determined from the sound pressure measured at any location of the duct cross section:

$$P = \overline{pv}S$$ Equation 1

where S is the cross-sectional area, and the overbar indicates time averaging.

In logarithmic form, the former equation reads:

$$L_w = L_p + 10\log\frac{S}{S_0} - 10\log\frac{\rho c}{(\rho c)_0}$$ Equation 2

where $S_0 = 1\,\text{m}^2$, $(\rho c)_0 = 400\,\text{Ns/m}^3$ are the usual reference values.

This formula applies for plane waves only, that is for frequencies below the cut-off frequency f_c, since at higher frequencies the sound pressure level is not homogeneous on a duct cross-section. For a circular section, the cut-off frequency writes:

$$f_c = 1.84 \frac{c}{\pi D_c}$$

Since $D_c = 0.18$ m, $f_c \approx 1100$ Hz

Barret and Osborne [2] showed that one may use the plane wave formula Equation 1 as an approximation, in the presence of higher modes, provided the sound pressure is measured at a suitable distance of the duct wall: For a directional sensor (like a microphone) equipped with a turbulence screen, the optimum radial position r is close to the duct wall, where the mode amplitudes are generally larger, to compensate with the microphone directivity [2].

According to the European norm [4], since $0.15 < D_c < 0.5$ (where D_c is the diameter of the duct where the measurement takes place) we need

$$2r/D_c = 0.8$$

According to the same European standard, for a given frequency bandwidth Δf we have

$$L_p(\Delta f) = 10 \log \left(\frac{1}{3} \sum_{i=1}^{3} 10^{\frac{Lp_i(\Delta f)}{10}} \right)$$

where Lp_1, Lp_2, Lp_3 are the sound pressure levels recorded by the microphones 1, 2, 3.

And finally the sound power reads:

$$L_w(\Delta f) = L_p(\Delta f) + 10 \log \frac{S}{S_0} - 10 \log \frac{\rho c}{(\rho c)_0} + C$$

Equation 3

The corrective factor C is given in annexe 1. It represents the global frequency response correction of the microphone and its turbulence screen.

$$C = C_1 + C_2 + C_3 + C_4$$

8

C_1: correction (in dB) provided by the manufacturer, which must be added to the response of the calibrated microphone in order to obtain the free field response.

C_2: Frequency response correction (in dB) of the turbulence screen as a result of a plane waves field in the direction of the axis of the probe.

C_3: Frequency response correction (in dB) of the turbulence screen as a result of the superimposed flow.

C_4: Modal frequency correction (in dB) which accounts for the fact that the sound pressure measured by a microphone with turbulence screen at the specified radial position does not give exactly the correct sound power in the duct when applying the plane wave formula.

2.4. Description of the inlet geometries

Seven different air inlet geometries were tested and are described in the following sections. The chosen geometries do not aim to be consistent with the inlets that are actually used in HVAC car systems. Basic geometries were used in order to characterise the effects of a bend (its length and its orientation regarding the scroll cut-off), a straight duct, a cross, and the sharpness of the intake.
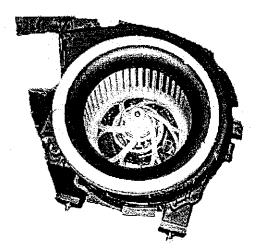

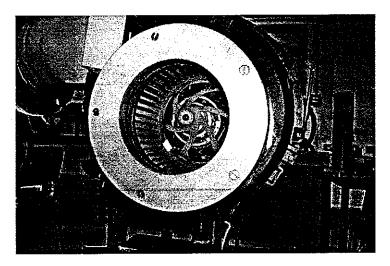Figure 6 – blower with no adapter (original configuration C1)

Figure 7 – Configuration 2: with adapter

2.4.1. no specific air inlet

The first configuration (Figure 6) is simply made of the blower itself, without any added inlet geometry. There is a build-in converging intake bringing the air flow inside the wheel.

2.4.2. Blower with adapter

An adapter had to be done in order to fix the inlet geometries to the blower. A sudden restriction of the inlet section occurs here because of the adapter, which has a 11 cm inside diameter (same as the external diameter of the used ducts and bends), compared to the 12 cm diameter of the blower's inlet.

The wooden ring is fixed on the top of the collar. There is no converging section, since this geometry was not meant to be tested, being just a linking item. However I decided to make some measurements with this configuration in order to compare it with the configuration without the wooden ring, which has a converging restriction.

2.4.3. Bend parallel to the fan outlet with a bell mouth

The third configuration is built with the blower, the adapter previously depicted, a 90° bend and a straight duct. A bell mouth shaped intake finally completes the whole. As shown on the picture (Figure 8), the inlet geometry is aligned with the blower outlet.

10

Figure 8 – Configuration 3: parallel bend with a bell mouth

Figure 9 – configuration 4: perpendicular bend with a bell mouth

2.4.4. Bend perpendicular to the fan outlet with a bell mouth

This configuration is very much similar to the precedent configuration: The exact same inlet geometry is used. The difference lies in the position of the inlet regarding the fan outlet: in this case the bend is oriented in a direction perpendicular to the fan outlet (Figure 9).

11

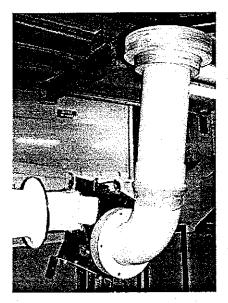The Configurations 3 and 4 are expected to give some insight on the influence of the scroll cut-off on aerodynamic and acoustic performances.

2.4.5. Straight duct with a bell mouth

The configuration 5 consists in a duct fixed to the blower via the adapter, and the bell mouth shaped intake which is fixed at the other end (Figure 10). The few distortions generated by the intake are phased inside the duct. The flow entering the wheel is likely to be homogeneous, with little distortions.
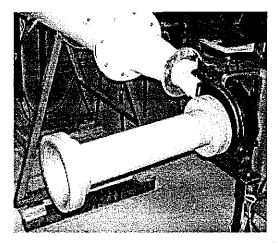

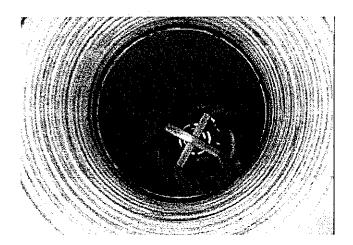Figure 10 – configuration 5: Straight duct with a bell mouth

Figure 11 – configuration 6: Straight duct with a cross and a bell mouth

2.4.6. Straight duct with a bell mouth and a cross

This configuration is similar to the previous one, except that a cross is placed very close to the blower inlet. Apart from the aerodynamic losses that this cross will create, and which depends on the cross size and width, the purpose of this configuration is to evaluate the effect of the cross regarding the sound power spectra: man may expect this cross to generate a noticeable tonal noise.

2.4.7. Short bend

A short bend is fixed in the same position as for the fourth configuration, that is perpendicular to the blower outlet. The difference between the two cases is the absence in the later of a duct and a bell mouth: The air enters directly into the bend with no converging section.

2.4.8. Short bend with a grid fixed at the intake

This eighth geometry should have been tested as well. It has not been the case because of lack of time. But it is very likely that the aerodynamic and acoustic performances of this geometry would have been even worse than those of the configurations 6 and 7 (cross in the straight duct and short bend).

3. Experimental results

3.1. Static pressure

3.1.1. Overview

Obviously the air inlet has a strong influence on the static pressure delivered by the blower. If we study the air inlets independently from the centrifugal fan, we will notice that they generate different pressure losses as well as different flow rates. For example it is well known that a straight duct will introduce less loss than a sharp bend. Therefore it is not a surprise to find that the ideal configuration from the aerodynamic point of view is the one without a specific air inlet.
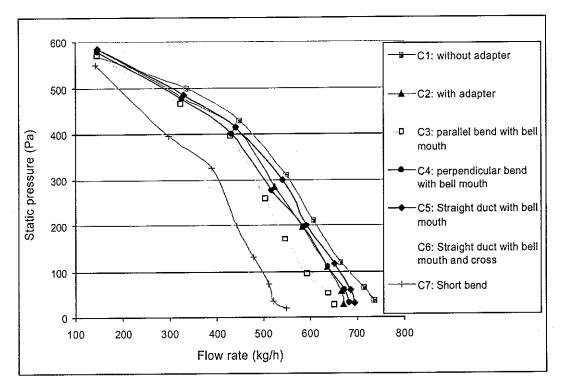
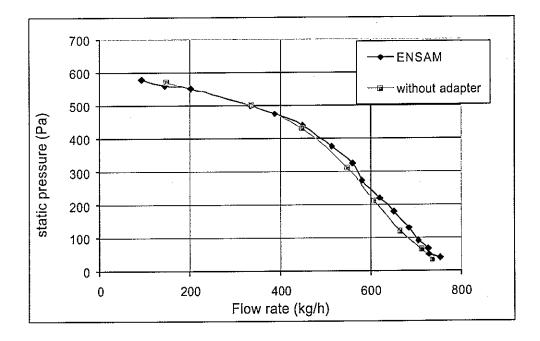Figure 13 – Static pressure as a function of the flow rate

Figure 12 – static pressure measured by the ENSAM, and with the configuration 1 (without adapter)

Experiments with the configuration without inlet were made previously for RENAULT at ENSAM, with the exact same rig and blower. Two ENSAM students indeed tested a few blowers during spring 2001 as part of a contract between ENSAM and Renault [6]. The results we obtain are very similar to those that ENSAM previously got (Figure 12).

3.1.2. Influence of the bell mouth

We could have thought the air inlet with a straight duct would cause more pressure loss than the air inlet with the adapter. It would perhaps have been the case if there was no bell mouth at the beginning of the straight duct: when the inlet with the adapter has a sharp edge, the duct starts with a smooth bell mouth, causing much less turbulences. The pressure loss due to the friction inside the duct is then almost insignificant compared to loss generated by the sharp adapter.

But the most significant influence of the bell mouth can be observed when comparing the curves for the three configurations with a bend: for the perpendicular and parallel bends, there is a bell mouth inlet, and the results are, at least in the perpendicular case, almost as
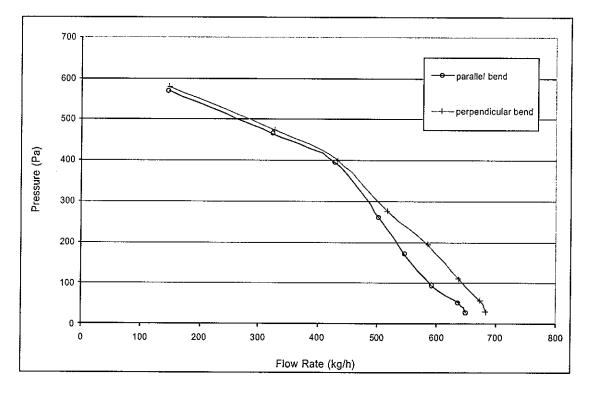

Figure 14- Static pressure with the parallel and perpendicular bends

15

good as with the straight duct. In the case of the short bend the flow enters the duct without any converging section, generating a huge pressure loss.

3.1.3. Influence of the direction of the bend

At low flow rates the two curves stay very close from each other. The configuration with the bend in the direction perpendicular to the fan output seems to be better at higher flow

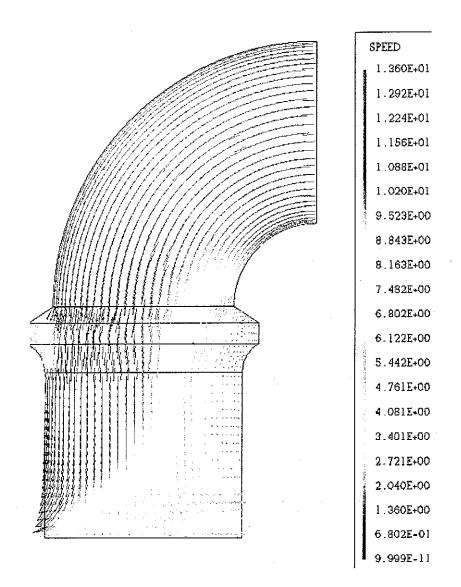| SPEED	
1.360E+01	
1.292E+01	
1.224E+01	
1.156E+01	
1.088E+01	
1.020E+01	
9.523E+00	
8.843E+00	
8.163E+00	
7.482E+00	
6.802E+00	
6.122E+00	
5.442E+00	
4.761E+00	
4.081E+00	
3.401E+00	
2.721E+00	
2.040E+00	
1.360E+00	
6.802E-01	
9.999E-11	

Figure 15 – repartition of the velocity field inside the wheel after a bend

16

rates.

The higher the speed in the bend, the more unbalanced the velocity field will be inside the wheel. Indeed, at high flow rates the flow will enter the wheel mostly from the opposite side of the bend, since the speed there will be higher than from the inside. Therefore with the "parallel" bend the flow will head straight toward the edge of the case (cut-off), where it will be driven back, producing a great flow rate loss. When the static pressure delivered with the two configurations looks more or less the same, the flow rates are clearly influenced by the orientation of the bend. Figure 15 presents the computed velocity field in the blower's wheel after bend. The computation was realized using the software CFX-Tascflow 2.11. The case is not taken into account here, since the outlet boundary condition (the flow rate) is set on the rotating cylinder representing the flow entering the wheel. This simple computation may help us to understand why the flow rate is reduced when the bend is aligned with the cut-off, although is does not show it: we obviously need to model at least the whole blower.

This example shows how the study of the inlet aerodynamic performances cannot be separated from the study of the blower's: If it may be an acceptable approximation as a first attempt to provide a convenient inlet geometry, the final solution should be defined by considering the ventilating system as a whole, since the several parts that compose the HVAC system interact with each other.

3.1.4. Aerodynamic recommendations

Amongst the seven tested geometries, the best results are given by the configuration 1, which is the basic configuration without adapter. The configuration 5 (straight duct with bell mouth) comes very close to it, but does not deliver the same flow rate and static pressure as with configuration 1, due to a slightly smaller inlet cross-section. The presence of a **bell mouth shaped intake** reduces noticeably the pressure losses, and the inlet of the configuration 2 (with the sharp edged adapter) generates a more important pressure loss via the sudden expansion that it induces.

The configurations 3 and 4 (perpendicular and parallel bends) generate some losses, although those stay small because of the presence of the bell mouth shaped intake as well as the existence of a duct between the intake and the bend. One has to **avoid if possible having the bend aligned with the blower's outlet**, because of the flow recirculation that

17

the scroll cut-off generates.

The configuration 7 accumulates two major misconceptions, in other words a short bend and an intake without a converging section. Taken separately they do not penalize the aerodynamic performances too heavily, but here both the static pressure and the flow rate drop dramatically.

Finally the cross placed in front of the wheel in the configuration 6 is probably too wide to be representative: the section is very much reduced by the presence of the cross, thus the static pressure and the flow rate generated by the blower are very poor.

3.2. Acoustic performances

3.2.1. Overview

The air inlets that were the worst from the aerodynamic point of view appear to be the worst as well concerning the sound power level, even though we kept the same voltage in
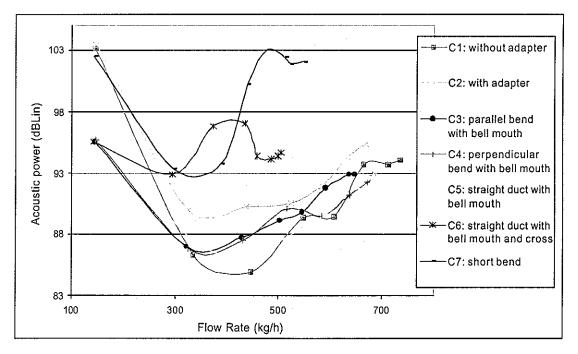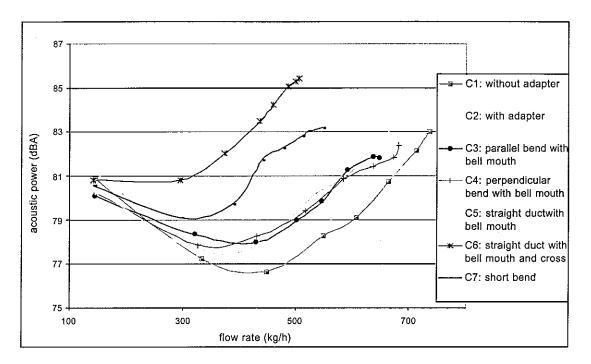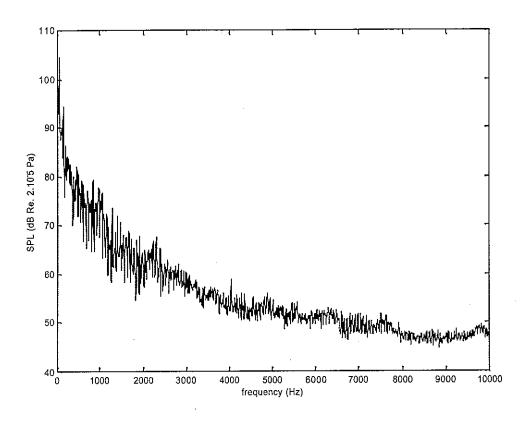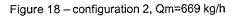

Figure 16 - Sound power

Figure 17 – Sound power level in dB(A)

all cases. If we increase the voltage in order to generate the same static pressure as for example the one we get for the configuration without any specific air inlet, then the acoustic properties will get even worse, since the sound power level increases roughly like the fifth power of the rotational speed.

Obviously the two configurations that are to be avoided are the configuration 6 and 7 (with the cross and with the short bend). They are not only awful from the aerodynamic point of view (low flow rate and static pressure), but concerning the acoustic performances as well.

The disturbed air inlet geometries introduce an inhomogeneous velocity field, which impinges the fan blades and therefore is expecting to create tones at the blade passing frequency and harmonics. In the facts that is not really was has happened, since only few configurations actually allowed us to see fan tones. The main component of the sound power is the broadband one. For example in the configuration 2 (with the adapter), the fundamental does not appear. The first harmonic (around 4000 Hz) can be noticed though (Figure 18).
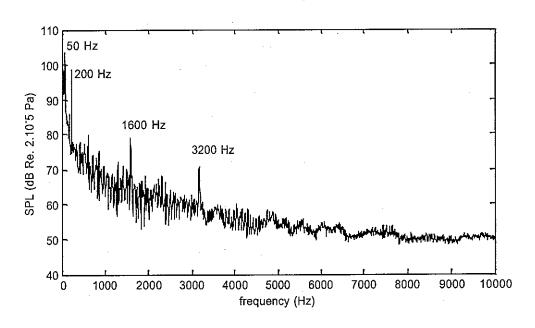
19

Figure 18 – configuration 2, Qm=669 kg/h

Figure 19 – configuration 1 (without adapter) at Qm=736kg/h

20

In the configuration 1 (without adapter) we obtain both the tone at the blade passing frequency (BPF) and the first harmonic), which are calculated as following:

$$f_0 = \frac{NB}{60} \qquad f_1 = 2f_0$$

B being the number of blades of the blower, and N the rotational speed (rpm)

We get as well a remarkable tone at 200Hz. It seems to come from the spokes of the wheel (6 spokes) and its frequency is therefore proportional to the rotational speed N of the blower:

$$f = \frac{6 \times N}{60}$$

This tone is visible at all flow rates for all the configurations, with often several harmonics. It may be interesting to take notice of it, although its influence on the global acoustic power is negligible when we apply the A-weighting filter.

The BPF and harmonics are visible for the other configurations at the low flow rates, but are hidden by the broadband noise at higher flow rates.
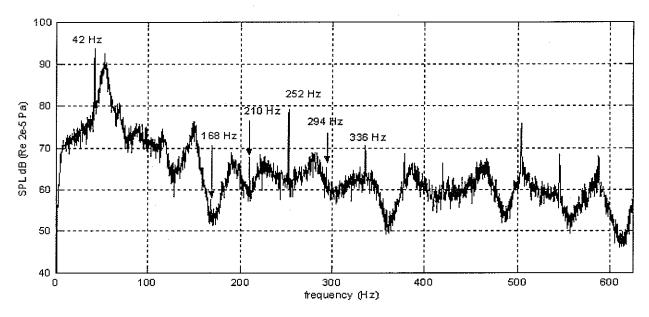

Figure 20 – Multiple pure tones (configuration 2, Qm=439 kg/h)

When the BPF and harmonics are not visible, there still remains a broadband noise, as well as a saw-toothed spectrum component (Figure 20).

The pure tones appear at multiples of the shaft rotational speed. The peaks that appear are very sharp and thin, do probably not come from aeroacoustic sources, but from the motor itself.

3.2.2. Influence of the bell mouth shaped intake

If the effects of the bell mouth were very much noticeable from the aerodynamic point of view, they become even more important concerning the acoustic performances:

- At the lower flow rate (around 145 kg/h) we can very clearly separate the seven configurations into two groups, depending whether the inlet geometry is provided with a bell mouth or not. Even the straight duct with the cross (configuration 6) is more silent than the configuration 1 at this low flow rate.

- At higher flow rates the effect of the bell mouth is still visible, since the acoustic power for the configuration 2 (with adapter) is higher than for the other configurations with the bell-mouth (except for the configuration 6 which has a bell mouth, but where the effect of the cross becomes probably more important as the flow rate increases).

The third octave spectra at the lowest flow rate (Figure 21) show that for the configuration 3 which has a bell mouth, the sound pressure level for the low frequency bands is much lower than for the configuration 1 which has a sort of bell mouth shaped intake, since the intake of the configuration 1 (blower with no specific air inlet) is made off a converging collar. The presence of a long straight duct between the intake and the blower (in the case of the configuration 3, the straight duct is placed between the intake and the bend) may be responsible for this difference at low flow rates.

The higher frequency bands on the other hand look very similar for all the configurations (for a same flow rate).
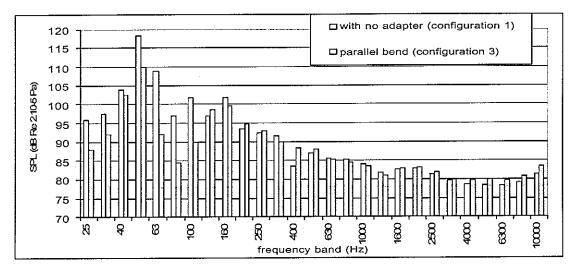
22

Figure 21 – Influence of both the bell mouth intake and the straight duct

The acoustic specifications at Renault are made taking into account the A-weighting. It is interesting to see that the differences at low flow rates are strongly reduced when expressed in dB(A): the A-weighting strongly reduces the influence of the low frequency third octave bands in the global acoustic power. Therefore the differences at a low flow rate between the geometries with or without a bell mouth shaped intake are not visible anymore.

The shapes of the seven curves (Figure 17) also look more similar one with another compared to the curves representing the acoustic power in linear decibels.

3.2.3. Influence of the corrective factor

The acoustic power is calculated by adding to each third-octave band (i) a corrective factor C_i (Cf. 2.3.2). This term is null for the low-frequencies, and becomes non-negligible for the frequencies beyond 1000Hz (Figure 22).
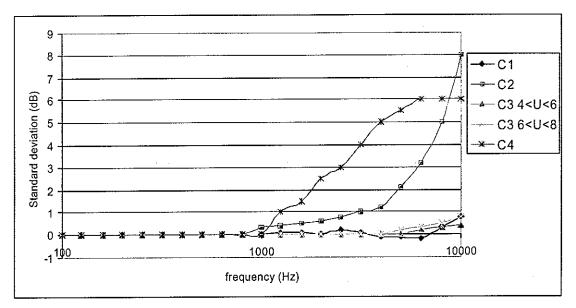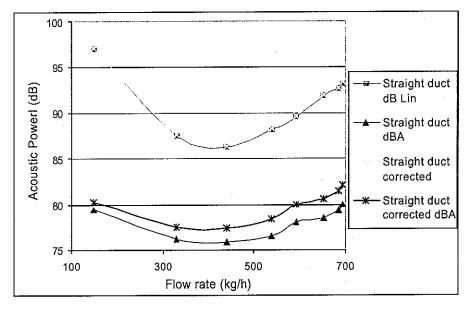
Figure 22 - Standard deviation

Figure 23 – Influence of the corrective factor on the global acoustic power

Since the acoustic power is mostly located in the low-frequency bands, the effect of the deviation from the sound power level is almost negligible. On the other hand when we apply the A-weighting the acoustic power at the low frequencies is cut down and the
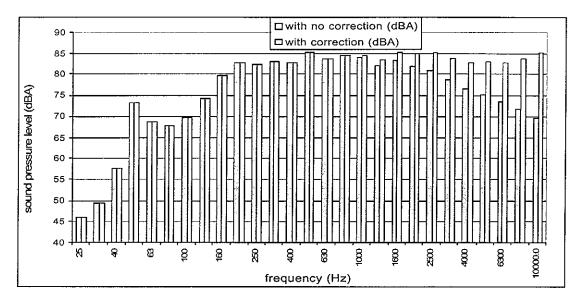
24

Figure 24 - third octave bands of sound pressure level for the straight duct (Qm=651kg/h) in dB(A)
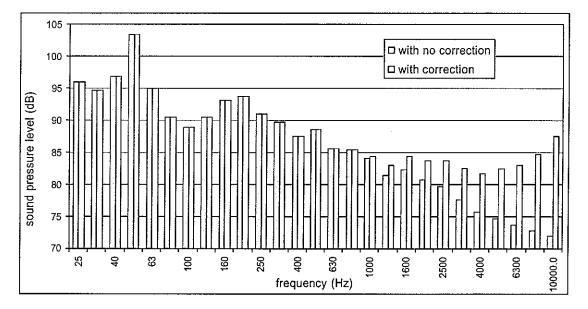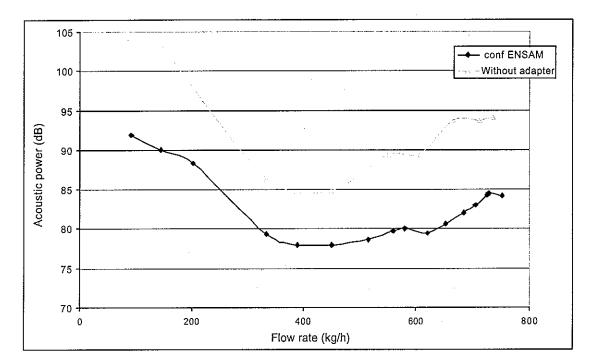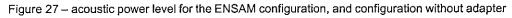

Figure 25 - third octave bands of sound pressure level for the straight duct (Qm=651kg/h) in dB

influence of the higher frequencies becomes visible. The correction effects are then amplified by the A-weighting.

3.2.4. Comparison with the experiments made at ENSAM

The experiments previously made at ENSAM give us acoustic results much lower than

Figure 27 – acoustic power level for the ENSAM configuration, and configuration without adapter
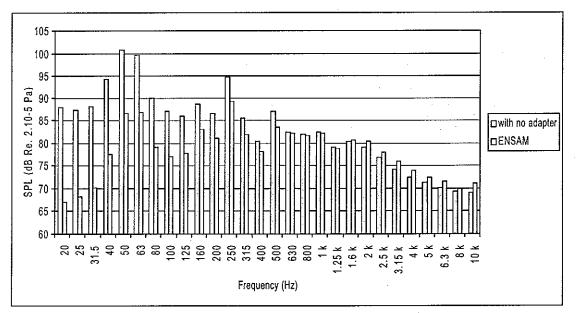

Figure 26 – Third octave spectra for the ENSAM/without adapter configurations (Qm=550 kg/h).No corrective factor C applied.

the ones we got for the configuration without adapter. The centrifugal blower was the same though, as well as was the fan rig, at the only exception of the acquisition card.

The third octave spectra of the two same configurations for a same flow rate show similar shapes, although the levels are not at all similar: for the low frequency third octave bands, the sound pressure level of the configuration 1 (without adapter) is about 20 dB higher than the level that ENSAM previously got. This gap gets lower and lower when the frequency increases, and is null around 1000 Hz. Then the tendency is reversed, and the ENSAM sound pressure level gets slightly higher (maximum of 2dB of difference at 10000Hz).

For the two third octave spectra showed (Figure 26) the corrective factor C was not taken into account, since it was not used for the internship at ENSAM in spring 2001.

Further experiments will be carried out at ENSAM in order to determine whether the acquisition card is responsible for this gap.

3.2.5. Incidence of the flow with the scroll cut-off

The figure below (Figure 28) suggests that the configuration 3 (bend parallel to the case output) is slightly worse than the configuration 4 (bend perpendicular to the case output). It is certainly true concerning the aerodynamic performances. But the differences that we observe for the acoustic power is mainly a consequence of these aerodynamic performances: The acoustic power levels are similar (the maximum gap between the two curves is 1 dB), although the flow rate is higher in the configuration 4. It is interesting to notice that the aerodynamic curves remain close to each other at low flow rates, and separate at higher flow rates: the influence of the scroll cut-off increases with the flow rate, as we already noticed (3.1.3).
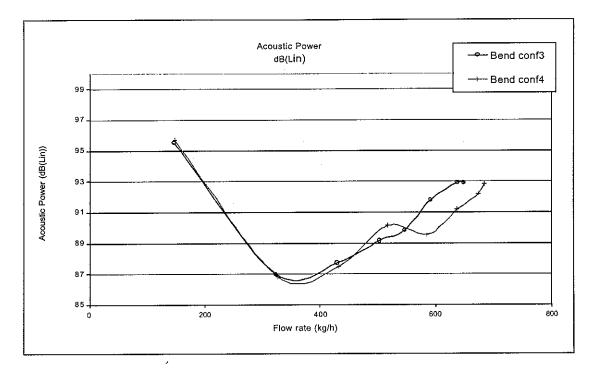
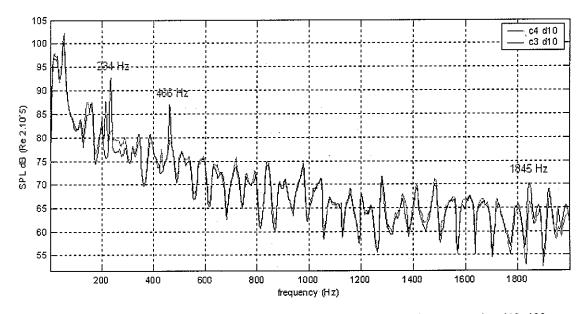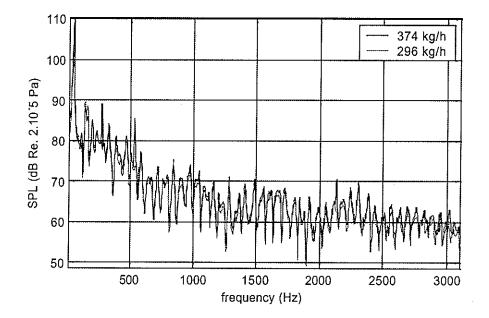Figure 28 – Acoustic power levels for the configurations 3 and 4

Figure 29 - SPL Spectra for the configurations 3 and 4 at the same diaphragm opening d10=180mm

When we compare the spectra of the two configurations for the higher flow rates, we can see that although the broadband noise remains very close in both cases, the level of the peaks is about 5 dB higher in the case of the configuration 3 (Figure 29), for which the

bend is aligned with the blower's outlet, therefore with the scroll cut-off. The fluid-structure interactions at the scroll cut-off generate dipole-like acoustic sources which produce tonal noises.

3.2.6. Influence of the cross

Theoretically the cross placed just in front of the wheel should interact strongly with the

Figure 30 – spectra for the configuration 6 at two different flow rates

Figure 31 - SPL configuration 6, Qm=374 kg/h

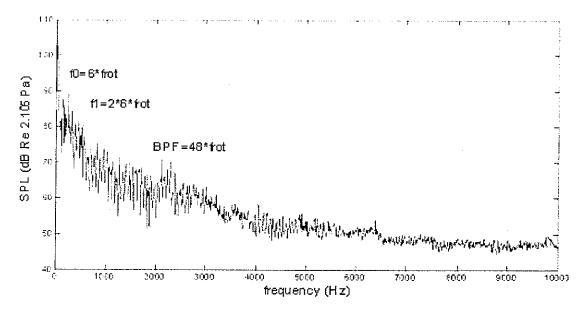blades of the wheel, as a stator would do with a rotor, although in this case the axe of the rotor is perpendicular to the axe of the stator.

When looking at the global sound power generated by the blower with this inlet (Figure 16) we observe that the shape of the curve differs from the others, since it presents a huge bump for the flow rates roughly between 300 and 450 kg/h. The comparison between the sound pressure level spectra at 374 kg/h and 296 kg/h for the configuration 6 shows (Figure 30) a gap of one to two decibels between the two curves, at the few exceptions of the tones, where there is a difference of five to ten decibels. Tonal noises arise at a flow rate where the efficiency of the blower is the best, and are responsible for this "bump".

Figure 31 shows the influence of the cross on the bowl: the four branches of the cross interact with the six strokes of the bowl, so that there is a peak at the frequency of the first harmonic of the bowl, that is twelve times the rotational frequency (the first common multiple between 4 and 6 is 12, therefore this frequency is likely to be excited).

3.2.7. Acoustic recommendations

On the contrary of an axial fan, a perturbation introduced in the blower through the air inlet is not likely to generate a tonal noise: although the inlet geometries produce flow perturbations, the flow field is so much turned upside down when entering the wheel, a lot of turbulence is generated and a high broadband noise arises, masking the tonal noise. Therefore the broadband part of the spectrum is responsible for the main noise. **Taking care of the aerodynamic constraints will often reduce this broadband noise, and solve a lot of the acoustics problems.** That is why we observe such a correlation between the static pressure and flow rate delivered by the rig, and the global in-duct sound power it generates.

The best configurations for the aerodynamic point of view, that is which deliver the highest static pressure and flow rate, are the configurations 1 (no specific inlet) and 5 (straight duct with a bell mouth). These sorts of geometries cannot be achieved in facts, especially because of a lack of space. The presence of a bend does not penalize very heavily the acoustic performances, as long as a proper intake is used: the combination of a bend with a bell mouth shaped intake proves to be quite efficient, especially compared

to the short bend alone, which should be avoided

4. Similarity laws

4.1. Acoustic similarity relationships for centrifugal fans

Neise [7] resumed the several similarity relationships used to establish a fan sound law. For a dimensionally similar fan series operating at the same point at the pressure head – volume flow characteristic, the total sound power W is proportional to the square of the static pressure difference ΔP_s, and to the volume flow Q:

$$W \propto \left(\Delta P_s\right)^2 Q$$

Equation 4

According to Neise [7], Madison was the first to establish this law in 1949. All empirical relationships are derived from this law. The above equation can be rewritten in terms of blade tip speed U_{tip} and impeller diameter D_2:

$$W \propto D_2^2 U_{tip}^5$$

Equation 5

The U_{tip}^5 dependence of the fan sound law agrees neither with the U_{tip}^4 dependence of free-field monopole radiation, nor with the U_{tip}^6 dependence of the dipole, nor with the U_{tip}^8 dependence of the quadrupole.

In addition, the assumptions that the aerodynamic flow through the rotor is similar for all the members of the series and that the effects of viscosity can be neglected have to be made to write down the equation 5. The first assumption alone makes this law unsuitable for this study, since the purpose of distorted inlet geometries is precisely to introduce an inhomogeneous flow in the rotor.

The law (Equation 4) cannot be used directly anyway, since the measurements have not been realised for the same operating points (i.e. for the same pressure heads and volume flows), but for the same voltage input. These laws of dimensional analysis are not

31

suitable to describe directly the air inlet effects.

4.2. Air inlet contribution

In order to describe the air inlet effects, one may compare two configurations (for example configurations 1 and 3), working on the same circuit (i.e. with the same diaphragm d placed at the output of the fan rig).

The configuration 1 is working at the operating point $(\Delta P_1, Q_1)$, and the configuration 3 is working at $(\Delta P_3, Q_3)$. For a same circuit, those two sets of operating points verify roughly:

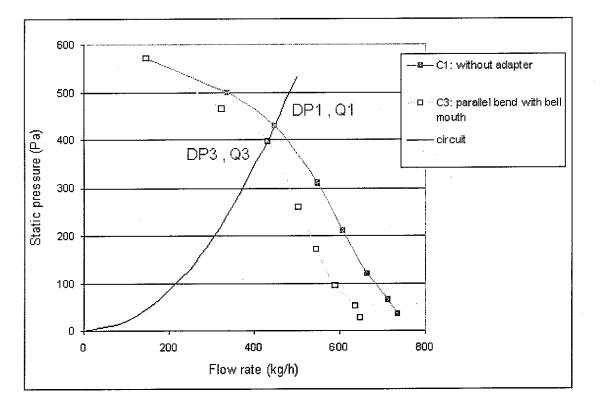$$\Delta P_s \approx K\ Q^2$$

Equation 6

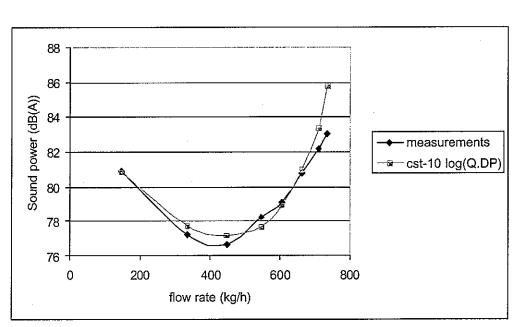Figure 32 - aerodynamic characteristics for configurations 1 and 3

where K is a constant that depends on the geometry of the circuit.

Finally one may notice that the acoustic power varies roughly like the inverse of the product $\Delta P.Q$, that is the aerodynamic power: indeed the acoustic power is actually a power loss, and one may consider the product of the acoustic power and the aerodynamic power to be constant:

$$W \approx \frac{A}{\Delta P.Q}$$

There is a good correlation between the estimated sound power for the configuration 1 using the above equation and the experiments (Figure 33). The gap between the two curves does not exceed 1 dB, at the only exception of the higher flow rates, where the gap reaches 3 dB.

Applying the same relationship to the configuration 3 gives:

$$W_3 \approx \frac{A}{\Delta P_3.Q_3}$$

Figure 33 - Sound power in dB(A) for the configuration 1

Equation 9

$$W_3 \approx W_1 \frac{\Delta P_1 \cdot Q_1}{\Delta P_3 \cdot Q_3}$$

Equation 10

$$W_3 \approx W_1 \left(\frac{Q_1}{Q_3} \right)^3$$

And finally:

Equation 11

$$LwA_3 \approx LwA_1 + 30 \log \left(\frac{Q_1}{Q_3} \right)$$

Therefore one can evaluate the sound power (in dBA) of the other configurations once one knows the sound power for the configuration 1, that is the configuration without any specific inlet geometry. Configuration 1 is a reference, that is used in order to describe the acoustic influence of the inlet geometry.
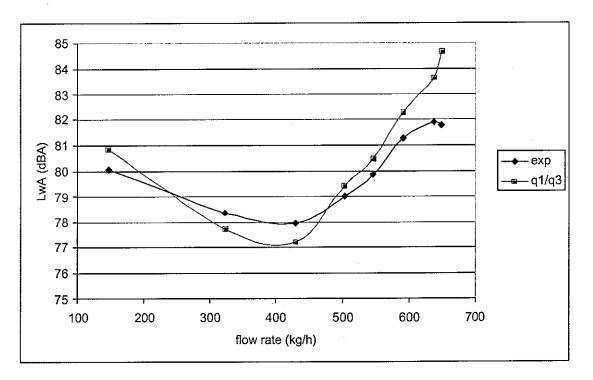

Figure 34 - Sound power in dB(A) for the configuration 3

34

The gaps that are observed for the configuration 3 look very similar to those observed for the configuration 1. There is a good agreement between the evaluation and the experiment, with a wider gap (around 3dB) for the higher flow rates.
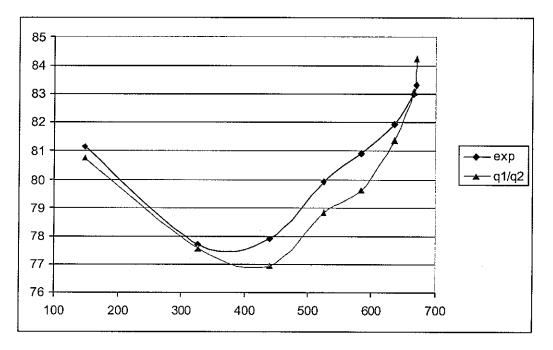

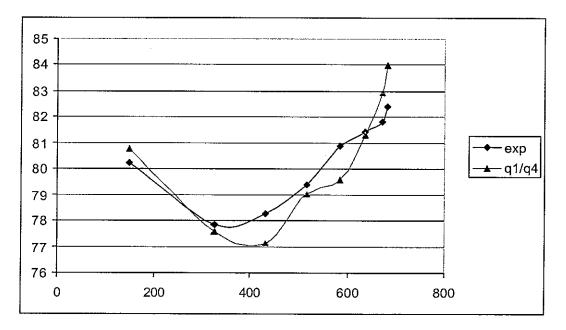Figure 36 - Sound power in dB(A) for the configuration 2

Figure 35 - Sound power in dB(A)
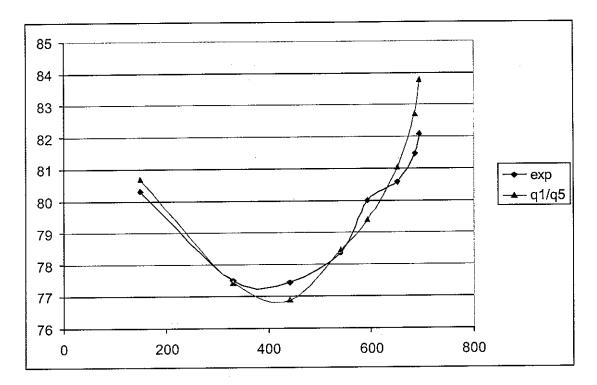
for the configuration 4

Figure 38 - Sound power in dB(A) for the configuration 5

Figure 37 - Sound power in dB(A) for the configuration 6

36
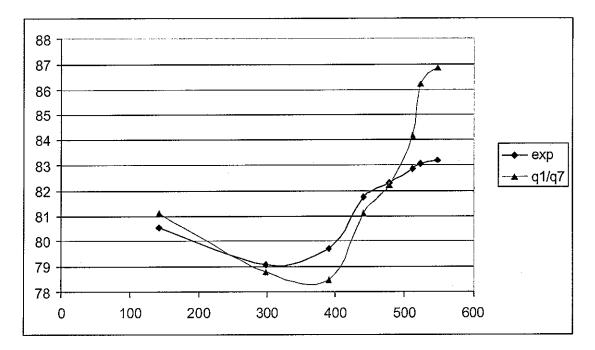
Figure 39 - Sound power in dB(A) for the configuration 7

There is a decent agreement for all the configurations, except for the configuration 6, that is the configuration with the cross. The shapes of the two curves differ rather obviously. Such a simple law cannot take into account all the mechanisms of the sound generation, and the influence of the cross previously described is one of them.

5. Conclusion and perspectives

The measurements at ENSAM allowed us to have a better understanding of the influence of the inlet geometry of an HVAC centrifugal blower on both the aerodynamic and acoustic performances of the later.

The static pressure and the flow rate delivered by the blower highly depend on the air inlet: any geometric disturbance lead to a pressure loss. There is a strong correlation between the aerodynamic performances of the system constituted by the air inlet and the blower and the A-weighted in-duct sound power it generates. The acoustic influence of the inlet geometry has been quantified through its aerodynamic performances, and a good agreement appears for most of the tested configurations.

The empirical relationship between the A-weighted acoustic power and the aerodynamic power has to be tested for several blowers, since only one centrifugal fan was used during the experiments at ENSAM.

Finally some experiments have to be done in order to understand the gap between the acoustic results obtained previously at ENSAM with an OROS acquisition card and those made in December with the Harmonie card.

38

References

[1] 01dB-Stell, HARMONIE measurement system. Getting started user manual.

[2] A.J. Barret, W.C. Osborne, "Noise measurement in cylindrical fan ducts", Journal of the Institute of Heating and Ventilating Engineers (1960) **28**, 308-318.

[3] W. Neise, F. Arnold, "On sound power determination in flow ducts", Journal of Sound and Vibration (2001) **244**(3), 481-503

[4] Norme Européenne EN25136, "Détermination de la puissance acoustique rayonnée dans un conduit par des ventilateurs (ISO 5136:1990 et rectificatif technique 1:1993)", Novembre 1993.

[5] Norme Française NF ISO 5801, "Ventilateurs industriels – Essais aérauliques sur circuits normalises", Décembre 1999.

[6] S. Carichon, F. Delamour, "Etude acoustique et aéraulique d'un pulseur automobile", Rapport Final PFE-ENG-01120, Juin 2001.

[7] W. Neise, "Application of similarity laws to the blade passage sound of centrifugal fans", Journal of Sound and Vibration (1975) **43**(1), 61-75

Appendix - Corrective coefficients C_1, C_2, C_3 and C_4

fqc	C1	C2	C3 4<U<6	C3 6<U<8	C4
20.00	0	0	0	0	0
25.00	0	0	0	0	0
31.50	0	0	0	0	0
40.00	0	0	0	0	0
50.00	0	0	0	0	0
63.00	0	0	0	0	0
80.00	0	0	0	0	0
100.00	0	0	0	0	0
125.00	0	0	0	0	0
160.00	0	0	0	0	0
200.00	0	0	0	0	0
250.00	0	0	0	0	0
315.00	0	0	0	0	0
400.00	0	0	0	0	0
500.00	0	0	0	0	0
630.00	0	0	0	0	0
800.00	0	0	0	0	0
1000.00	0	0.3	0	0	0
1250.00	0.1	0.4	0	0	1
1600.00	0.1	0.5	0	0	1.5
2000.00	0	0.6	0	0	2.5
2500.00	0.2	0.8	0	0	3
3150.00	0.1	1	0	0	4
4000.00	-0.1	1.2	0	0	5
5000.00	-0.1	2.1	0	0.2	5.5
6300.00	-0.2	3.2	0.2	0.3	6
8000.00	0.3	5	0.3	0.5	6
10000.00	0.8	8	0.4	0.8	6

40